Paper

Motor Performance Investigation of an Indirect Matrix Converter with a Reactor Free Boost Converter

Goh Teck Chiang* Student Member
Jun-ichi Itoh* Member

Abstract— This paper describes a three-phase power converter, which utilizes the neutral point of an induction motor, and demonstrates the motor performance of the proposed method under various operating conditions. Several motor test results, such as the speed-torque characteristic, the torque impact and the acceleration-deceleration characteristic, are included to confirm the performance of the induction motor. The structure of the proposed circuit consists primarily of an AC/AC converter (indirect matrix converter (IMC)) and a boost converter connected to the neutral point of the induction motor. In addition, this paper also proposes a method to reduce the ripple found in the battery current. Several experimental results showed that the motor works well, and even the leakage inductance is utilized in the boost converter.

Keywords: Indirect Matrix Converter, Boost Converter, Induction Motor, Neutral point of the motor, Pulse Width Modulation

1. INTRODUCTION

Hybrid electric vehicles (HEVs) are one of the promising fuel efficiency vehicles that are targeted to supply 20% of the total number of vehicles in Japan by 2020. The research on HEVs has proven this vehicle is able to reduce 48% of the CO_2 emissions released in traditional vehicles. Therefore, the known issues in HEVs that are now actively studied are cost, size, battery technical issues and high reliability of the electric motor.

The direct type of AC/AC converters has shown advantages in both size and cost. Matrix converters formed by nine bidirectional Reverse Blocking Insulated Gate Bipolar Transistors (RB-IGBTs) can deliver output voltage at variable frequency without electrolytic capacitors as storage devices [1]-[3]. However, the lack of a flexible connection to the DC link voltage in this converter is a problem for connecting a secondary source such as batteries. In Ref. [4], it is shown that an extra inverter circuit is required for connecting the DC link voltage to the matrix converter. Consequently, the size and cost would increase due to the extra use of the components.

In contrast, the indirect (two-stage) matrix converter (IMC), which also is a direct type of AC/AC converter constructed by a current source inverter (CSI) and a voltage source inverter (VSI), has a stable DC link voltage that can be connected to an extra source [5]-[7].

The authors previously proposed an AC/DC/AC circuit applicable in the HEV system [8]. The proposed circuit greatly reduced the size of the converter by removing two passive components, the electrolytic capacitors and the boost reactor, by utilizing the leakage inductance of the motor at the connection of the neutral point. In addition, the proposed circuit successfully demonstrated the fundamental operation of good converter performance.

However, the leakage inductance of a motor varies according to the structure of the motor. This variation results if the battery current consists of a ripple due to insufficient leakage inductance. Therefore, more research is needed to investigate and confirm the stability and performance of the motor.

In this paper, the authors propose a simple pulse-width modulation (PWM) method that generates a high switching frequency to reduce the ripple in the battery without adding additional hardware. The high-frequency switching method is only applied to the secondary side of the proposed converter.

Furthermore, the performance of the connection of the neutral point to the proposed circuit in a 750 W induction motor is also examined in this paper. The stability and the performance of the induction motor are investigated in an experiment. The experimental results, which clarify the speed-torque curve, the torque impact characteristic, and the acceleration-deceleration characteristic, prove the validity of the proposed method.

2. CIRCUIT TOPOLOGY

Fig. 1 shows the IMC circuit structure with the DC link part connected to a DC power source by a DC boost converter [8]. The boost converter also connects to the neutral point of the motor and utilizes the leakage inductance of the motor as a boost reactor.

Fig. 2 illustrates the energy flow diagram of the proposed circuit. In a hybrid system that has two power sources, a generator and batteries, the proposed circuit is capable of operating in three modes. The three modes are as follows: standard mode $P_{in}= P_{gen}$,

* Nagaoka University of Technology
1603-1, Kamitomioka-machi, Nagaoka 940-2188

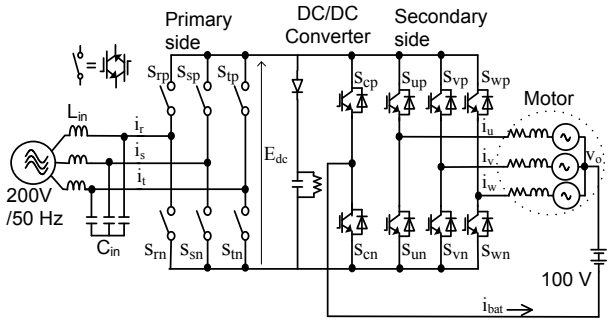

Fig. 1 Proposed circuit topology.

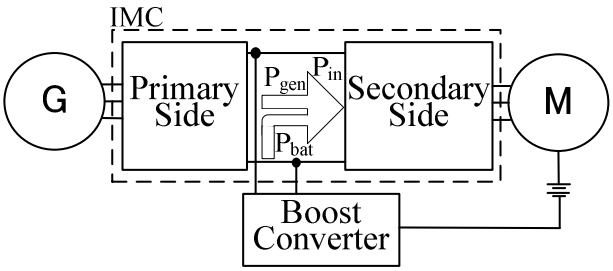

Fig. 2 Proposed circuit energy flow diagram.

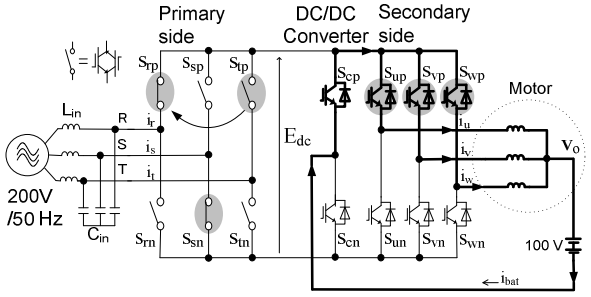

Fig. 3 Operation of the boost converter during the zero vectors.

electric vehicle (EV) mode $P_{in} = P_{bat}$, and hybrid electric vehicle (HEV) mode $P_{in} = P_{gen} + P_{bat}$. In these modes, P_{in} =input power, P_{bat} = battery power, P_{gen}, = generator power.

The operation of the boost converter depends on the zero vector periods of the inverter side. The battery current is charged through the motor leakage inductance at every zero vector period. Fig. 3 shows the equivalent circuit of the zero phase sequence. The upper arms of the inverter (S_{up}, S_{vp}, S_{wp}) are considered as one arm during the zero vector periods. The output currents flow within the inverter side, and the DC link current is zero. The primary side achieves the zero current switching (ZCS) during this zero vector period, as shown by the shaded switches in Fig. 3. The charge mode operation of the boost converter is shown in Fig. 3. In the charge mode, the battery current flows into the inverter arms and then to the leakage inductance of the motor.

3. PROPOSED CONTROL METHOD

3.1 Conventional Control Method

Fig. 4 shows a control block diagram of the proposed circuit, which is based on the carrier comparison method. The primary side uses single-phase modulation (Single phase Mod. in Fig. 4) and includes a pulse pattern conversion to convert the voltage source switching patterns into the current source [9], where i_r*, i_s* and i_t* represent the input current commands. The conversion technique of the single-phase modulation is explained in Ref. [9].

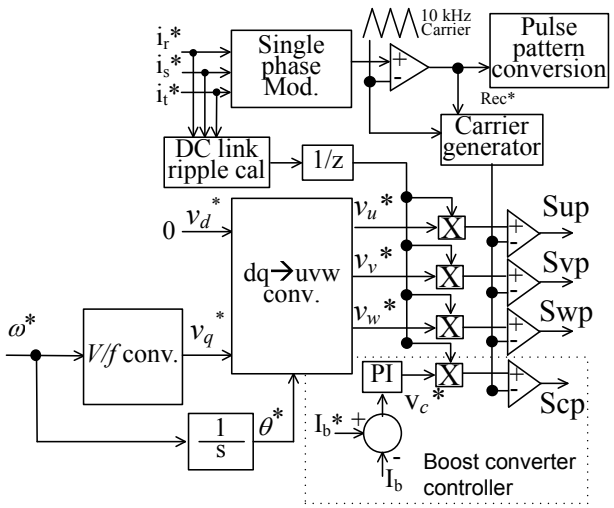

Fig. 4 Control block diagram.

The principle is to control the three-phase input voltage so that the input voltage carrying the maximum phase voltage is always selected; this selection corresponds to a switch that is always turned on. Then, the other two legs consisting of the medium phase voltage and the minimum phase voltage are in the switching state. The pulse pattern conversion is a simple logic selector that converts the voltage source PWM pulse pattern into the current source PWM pulse pattern. For example, if S_{rp} contains the max-phase voltage, S_{rp} = On, S_{sp} and S_{tp} = Off at the upper arm, and S_{rn} = Off at the lower arm. Here, S_{sn} and S_{tn} are the switching of the negative phase of the S phase and the T phase input voltages, which are at the med-phase voltage and the min-phase voltage, respectively. By applying this technique, a DC link voltage is formed that contains a frequency ripple with six times the input frequency.

A carrier generator that can produce a variable carrier based on the primary side command (Rec*) is used in the secondary side and the boost converter side. The secondary side includes a *V*/f conversion to control the motor frequency and output voltage as constant values [10]-[11]. The motor speed is adjusted proportionally to the output frequency. Then, the magnetizing current of the induction motor remains practically constant in a wide adjustment range.

The boost converter controller contains a PI control for control of the battery current, and then PI gain value is multiplied by the DC link frequency compensator to obtain the desired switching pattern. In Ref. [8], it is explained that the boost converter operates at every zero vector output of the inverter side.

3.2 Limitation of the Boost Converter Operation

Since the boost converter operating principle depends on the inverter stage, the boost converter must apply the same type of carrier and the same frequency. One known limitation of this method is that the value of the inductance cannot be selected because the leakage inductance corresponds to the motor structure. Leakage inductance that is too small causes a high ripple in the battery current. To overcome the high ripple, a higher switching frequency must be applied.

In addition, the application of this boost converter in the IMC results in an inconstant switching duty ratio of the boost converter. The secondary side of the IMC uses an inverter carrier that has a frequency that is two times higher than that of the original carrier.

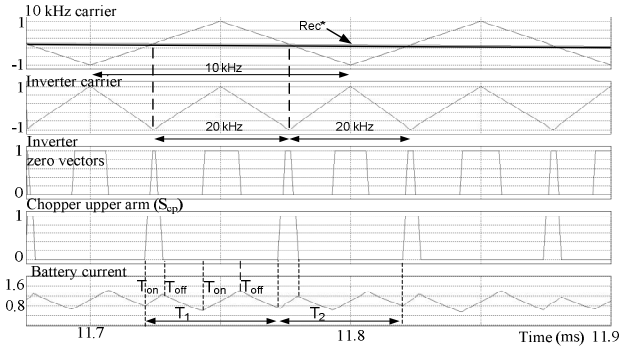

(a) Rec*=0.5.

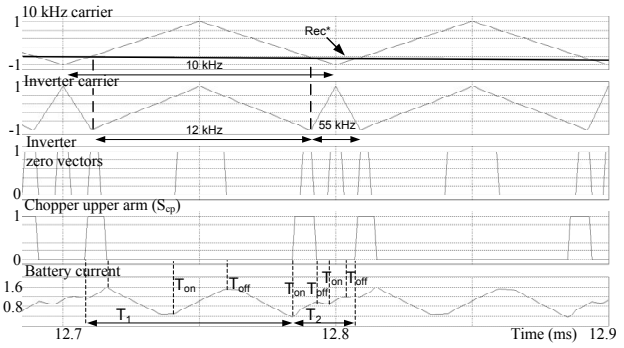

(b) Rec*= 0.2

Fig. 5 Increase of the battery current ripple due to the inconstant primary command Rec*.

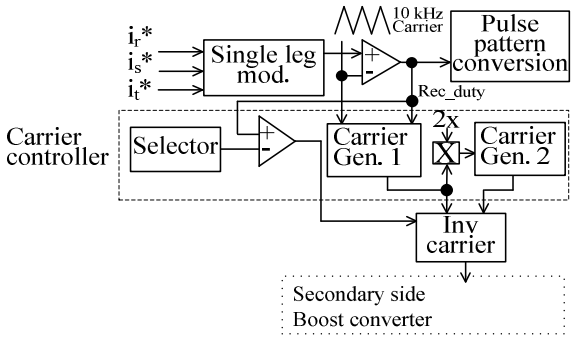

Fig. 6 Modification of the carrier controller in the control block diagram.

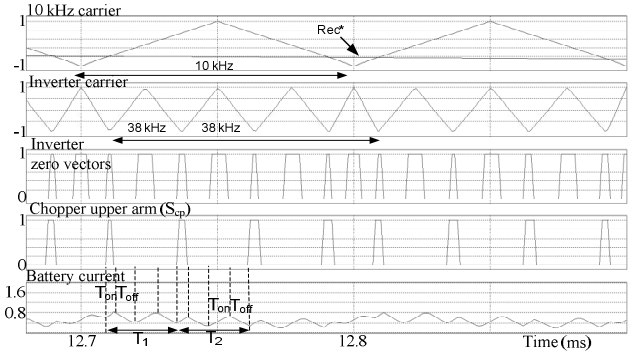

Fig. 7 Suppression of the battery current ripple with the proposed control. (Rec*=0.2)

The offset value of the inverter carrier is adjusted according to the cross point of the primary side command and the normal carrier. With this method, the switching periods for the zero vectors vary from one point to another. This phenomenon can be seen from the carrier waveforms in Fig. 5. As a result, the battery current ripple increases due to the inconstant primary command.

TABLE I. SIMULATION PARAMETERS

Input voltage	200 V
Input frequency	50 Hz
Carrier frequency	10 KHz
Output frequency	35 Hz
DC source	100 V
Leakage Inductance	5 mH

Fig. 5(a) and Fig. 5(b) show the simulation results of the battery current ripple subjected to the inverter carrier. In Fig. 5(a), the primary command (Rec*) is located at the middle range of the original carrier. The inverter carrier is formed with the same duty per cycle, at approximately 20 kHz. The zero vector periods can be considered constant in this range. From this figure, time T_1 is nearly equal to T_2. The chopper upper leg is switched on at every 20 kHz at the same time as that of the upper arm zero vector periods. During the On-state (T_{on}), the battery current increases, and it decreases during the Off-state (T_{off}).

In Fig. 5(b), Rec* is at the minimum range or the maximum range of the original carrier (Rec* =0.0→0.2 or 0.8→1.0). In these areas, the inverter carrier per cycling is not at the same frequency. Hence, the zero vector periods are inconstant, as shown between T_1 and T_2 of Fig. 5(b), and it can be stated that T_1 is not equal to T_2. The battery current increases sharply during time T_1. Until time T_2, the battery current cannot be released because the On-state and Off-state occur too rapidly. These periods cause the large ripple.

The following detail must be noted: an individual switching frequency that is different from the frequency of the inverter carrier cannot be applied for the boost converter. If the switching pattern of the boost converter fails to synchronize with the zero vectors, the ripple is larger due to the incorrect switching timing.

3.3 Proposed Carrier Comparison Method

Fig. 6 shows the proposed control block diagram for eliminating the ripple in the battery current. If we only increase the inverter frequency, the switching loss increases. Therefore, a new inverter carrier that includes a limiter is introduced to eliminate the current ripple in the selected zone only. The unselected zone remains the same as that of the conventional carrier.

Compared with the conventional control diagram, all parts in the proposed control diagram except the carrier controller are the same. The inverter carrier is combined with carrier generator 1 and carrier generator 2 to output a new inverter carrier. Carrier generator 1 carries two times the frequency of the original carrier, which is the inverter carrier from the conventional method, as described in Section 3.2. Carrier generator 2 can double the frequency of carrier generator 1. Carrier generator 2 uses a fixed point duty command so that at every cycle an approximately two-times higher frequency is generated. The symbol “2x” in Fig. 6 represents this multiplier. Then, these two carriers are sent to the block controlled by the selector signal.

The selector decides whether carrier 1 or carrier 2 is the output carrier for the boost converter controller and the secondary side controller. The comparator, based on the comparison between the selector and Rec*, is used to distinguish the zone. That is, when Rec*= 0–0.25 or Rec*= 0.75–1.0, the comparator outputs signal

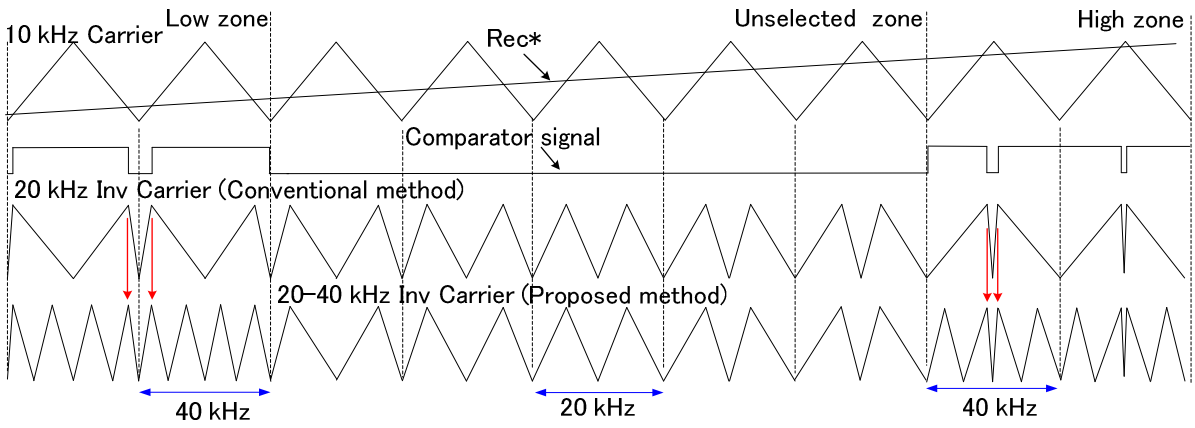

Fig. 8 Diagram explanation for the proposed control method.

"1" and carrier 1 is applied in this zone; thus, this zone is known as the selected zone. However, when the unselected zone is within Rec*= 0.26–0.74, the comparator outputs signal "0" with carrier 1.

Fig. 7 shows the switching pattern for the selected zone. This figure uses the same period and condition shown in Fig. 5(b). It can be seen that at time T_1=T_2, the battery current is well under control. The zero vector periods are occurring constantly and the battery ripple can be greatly reduced.

Fig. 8 explains the characteristics of the new inverter carrier. At the top is the original 10-kHz carrier and Rec*. The second pattern is the comparator signal. The third is that of the inverter carrier from the conventional method (20 kHz). The last is the pattern of the proposed inverter carrier.

Each cycle of Rec* is separated into the selected zone and the unselected zone, as previously discussed. The selected zones are the low zone within 0.0–0.25 and the high zone within 0.75–1.00. When the comparator is "1" in the selected zone, a new carrier having a double inverter frequency is used (40 kHz). When the comparator is "0" in the selected zone, the same frequency of the original carrier is copied into the new carrier. These frequencies are used because these areas are too narrow to create a new carrier.

The unselected zone is applied with the conventional carrier, and the same frequency carrier is brought into the new carrier. As a result, a new inverter carrier containing 20 kHz and 40 kHz frequencies is formed. When the inverter carrier reaches the inconstant zone, the 40-kHz constant carrier takes over. This method ensures the constant switching of the zero vectors for the selected zone.

4. SIMULATION RESULTS

Table I shows the simulation parameters. Fig. 9 shows the simulation results using the conventional type of inverter carrier. The battery current contains a large ripple and also affects the inverter currents. It is known from Ref. [8] that the inverter current contains one-third of the battery current as a zero-phase sequence component. Therefore, the total harmonics distortion (THD) value of the output current is influenced by the battery ripple.

Fig. 10 shows the simulation results using the proposed method. Note that the ripple of the battery current is greatly reduced. The selectors are set in the range of 0.0–0.25 and 0.75–1.00 in this simulation. The zone declaration can be clearly seen from the inverter carrier. The darker side represents the 40-kHz carrier and the lighter side represents the 20-kHz carrier. The new inverter did not affect the performance of the system and yet further reduced the THD value of the output currents.

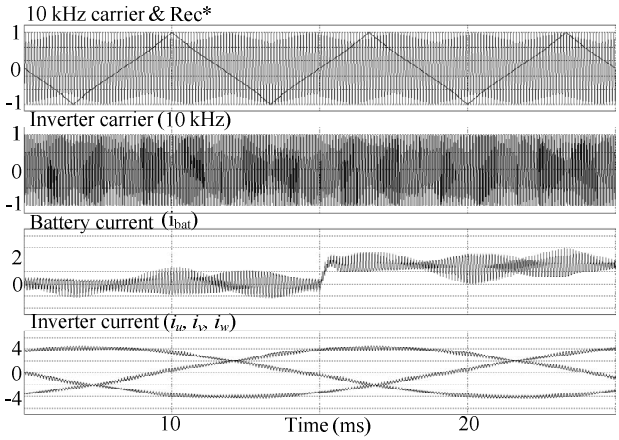

Fig. 9 Simulation result with the conventional carrier.

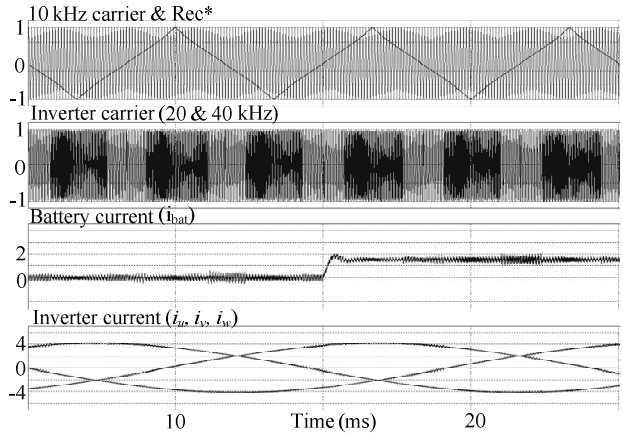

Fig. 10 Simulation result with the proposed carrier.

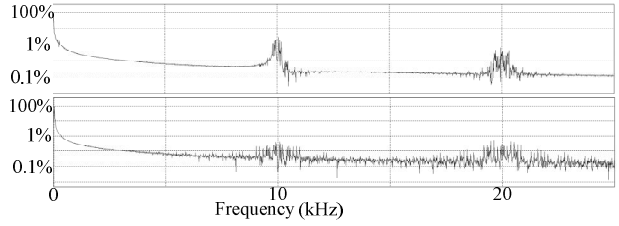

Fig. 11 Harmonic analysis for the output current (i_u).

Fig. 11 shows the harmonics analysis for the output current (i_u). The top pattern is the conventional method and the bottom one is

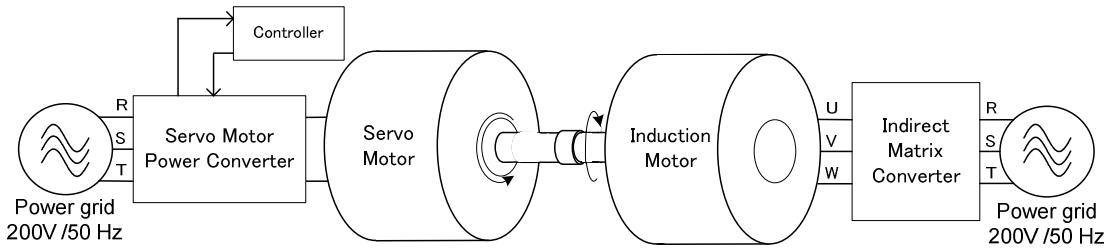

Fig. 12 Motor experimental setup.

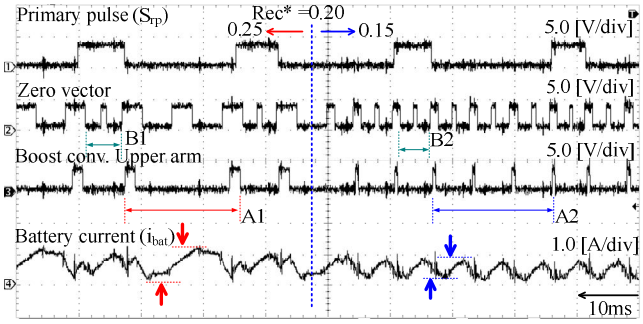

(a) Rec*=0.15-0.25.

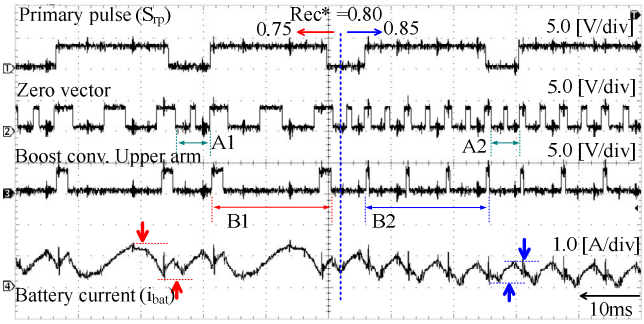

(b) Rec*=0.75-0.85.

Fig. 13 Relations between the zero vector pulses and the battery current ripple with the proposed method.

the proposed method. At 10 kHz, the 2nd harmonic component of the proposed method is less than that of the conventional method. This result indicates that the THD of the output current is improved.

5. EXPERIMENTAL RESULTS

The first subsection of this section discusses the experimental results of the ripple reduction in the battery current, the second section shows the adjustable speed drive performances with the three-phase induction motor used in the proposed circuit, the third shows the torque impact, and the fourth the acceleration-deceleration characteristic. The motor performances are investigated based on the control block diagram in Fig. 4.

Fig. 12 shows the setup between the induction motor and the load generator, which uses a servo motor. Table II shows the parameters of the induction motor and the servo motor. The servo motor provides the motor load. The torque sensor and the speed sensor are located at the servo motor. The induction motor is powered by the indirect matrix converter, and the servo motor is directly connected to the grid. A controller is attached to the servo motor to control the torque directly. The speed and torque data are obtained from the controller for monitoring purposes.

TABLE II. MOTOR PARAMETERS

Induction motor (Fuji: MLH6085M)			
Motor Power	750 W	Poles	4/ 50 Hz
Rated Voltage	200 V	Rated RPM	1420
Rated Current	3.6 A	Leakage inductance	4.42 mH
ES Servo motor (Fuji: GRK1151A)			
Motor Power	1500 W	Rated RPM	2000
Rated Votlage	200 V	Rated Torque	7.16 N.m
Rated Current	8.6 A	Max Torque	10.8 N.m

TABLE III. EXPERIMENTAL PARAMETERS

Input voltage	200 V	LC Filter Cut-off frequency	2.4 kHz
Input frequency	50 Hz	DC source	100 V
Carrier frequency	10 kHz	Measured leakage inductance	4.42 mH
Variable carrier frequency	20 kHz	Output frequency	10 Hz – 45 Hz

Table III shows the experimental parameters. The verifications are classified into three sections: the speed and torque curve, the torque impact characteristic, and the acceleration and deceleration characteristic.

5.1 Ripple Reduction in the Battery Current

Fig. 13(a) and Fig. 13(b) show the experimental results in the case that the primary command (Rec*) is 0.15–0.25 and 0.75–0.85, respectively. In these two figures, the top result shows the primary command pulse according to Rec*, the second shows the zero vector pulse, the third is the switching pulse of the chopper upper arm, and the last is the battery current. In Fig. 13(a), Rec* is located at the low peak of the inverter carrier. The selected zone is set to start at Rec*=0.20, which is represented by the dotted line in the middle of the figure. As can be seen from this figure, the battery current contains a high ripple at the unselected zone. The inverter carrier changes immediately once Rec* reaches 0.20, and the zero vector periods occur rapidly. A1 and A2 in Fig. 13(a) show the periods where the carrier is larger than Rec*. B1 and B2 in Fig. 13(b) show the periods where the carrier is smaller than Rec*. Comparing periods A1 and A2, the zero vectors in period A2 are approximately twice those in period A1 due to the use of the 40-kHz carrier. Notice that the conventional 20-kHz carrier is applied in periods B1 and B2. As a result, the amplitude of the ripple is reduced.

Fig. 13(b) shows the result in the case that Rec* is located at the peak of the inverter carrier. The frequency of the inverter carrier

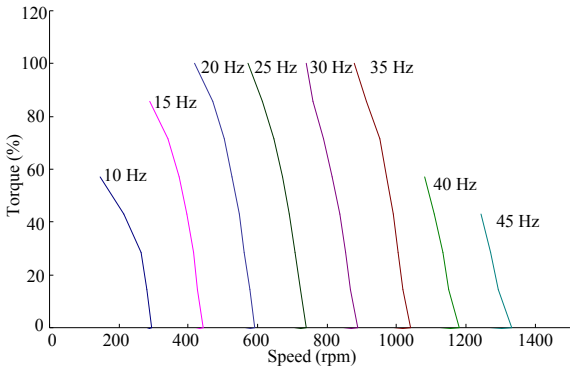

(a) Indirect matrix converter.

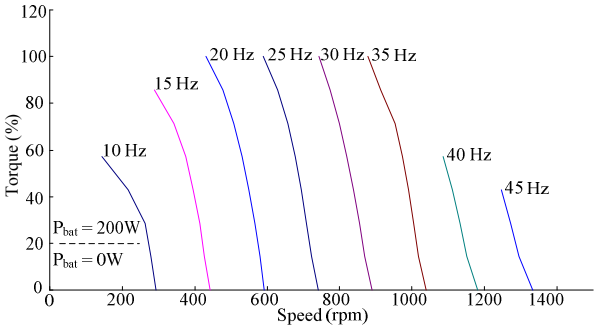

(b) Proposed converter.

Fig.14 Speed and torque characteristic of the induction motor.

changes to 40 kHz immediately after Rec* is 0.80. In the unselected zone (Rec* < 0.80), the amplitude of the ripple is high due to the inconstant switching period. However, in the selected zone (Rec* > 0.80), the ripple is reduced because of the high switching frequency and constant switching duty ratio. The definitions of A1, A2, B1 and B2 are the same as those for Fig. 13(a). Notice that the sequence of the zero vector in period B2 increases more than that in period B1. In both (a) and (b), the ripple is approximately reduced by 42%.

5.2 Speed and Torque Curve

Fig. 14 shows the relationships between the speed and torque characteristics of the induction motor. Fig. 14(a) shows the motoring data in the case that only the IMC is connected. Note that the *V/f* control is applied at all times. This graph shows good control over the induction motor. The reason the speed is not constant to the torque is because the induction motor contains slip according to the load torque.

Fig. 14(b) shows the relationships between the speed and torque characteristics of the proposed circuit connected to the induction motor. The battery current is pre-set at 0 A when the torque is below 20%. When the torque is 20% or larger, the battery current increases to 2 A. At an output frequency of 35 Hz, the torque is 100%, and the motor speed is 879 rpm. Likewise for the IMC connection under the same output frequency, the torque is 100%, and the motor speed is 877 rpm. The data in these two graphs show no difference, even at the neutral point of the motor connected to the boost converter. That is, the motor with the proposed converter runs in good operating condition.

Note that at 40 Hz and 45 Hz, the torque cannot reach 100% because of the limitation of the output voltage transfer ratio of the IMC. The output voltage transfer ratio of the IMC is limited to 0.866 of the input voltage. Moreover, the proposed circuit must

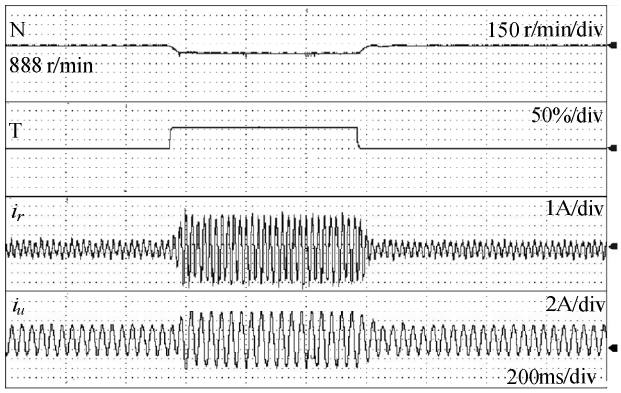

(a) Indirect matrix converter.

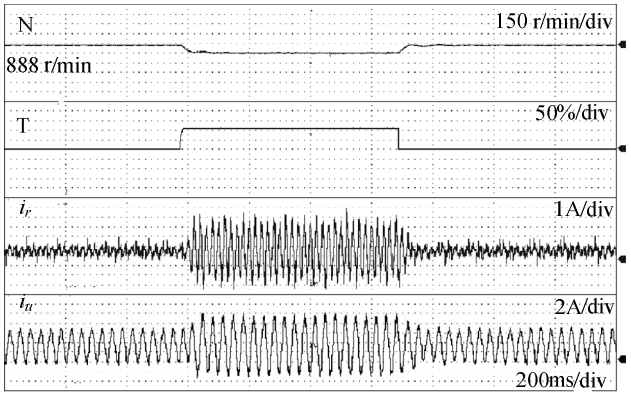

(b) Proposed circuit in EV mode. (P_{bat} =200 W)

Fig. 15 Torque impact characteristic of the induction motor.

apply three-phase modulation in the secondary side in order to generate the zero vector periods. This further reduces the voltage transfer ratio from 0.866 to 0.75. Therefore, starting at the output frequency of 37.5 Hz, the output voltage is not sufficient to deliver the power response to the torque.

5.3 Torque Impact Characteristic

This section demonstrates the torque impact characteristic under the EV mode and the normal mode, as shown in Fig. 15. Fig. 15(a) shows the normal mode operation, in which the boost converter is not connected to the motor and only the IMC is operating. The output frequency is 30 Hz, and the step increase of the torque is 100%

In Fig. 15(a), input current i_r shows an unbalanced sinusoidal waveform due to the low input power, which is nearly 170 W. As the torque increases to 100%, the input power immediately produces more power to maintain the speed. The output current i_u shows a good sinusoidal waveform at all times

The performance of the motor under the EV mode is shown in Fig. 15(b). The experimental condition is the same as that in Fig. 15(a). The battery power is 200 W at all times, and the input power is nearly 50 W; therefore, i_r shows poor waveform quality due to the low input current. When the torque increases to 100%, the battery power is maintained at 200 W and the input power eventually increases to maintain the motor speed. The input current i_r shows an unbalanced phenomenon due to the low input power, because the total input power is partially supplied by the secondary power. The output current i_u demonstrates a good sinusoidal waveform at all times, which matches the result in Fig. 15(a).

5.4 Acceleration and Deceleration Characteristic

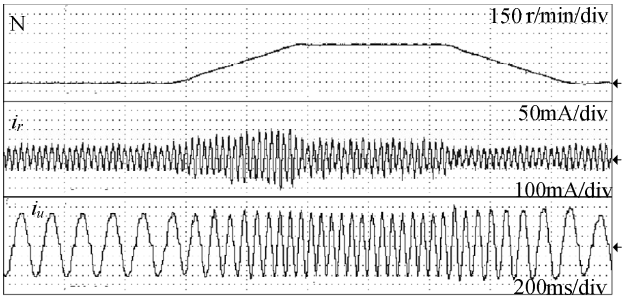

(a) Indirect matrix converter.

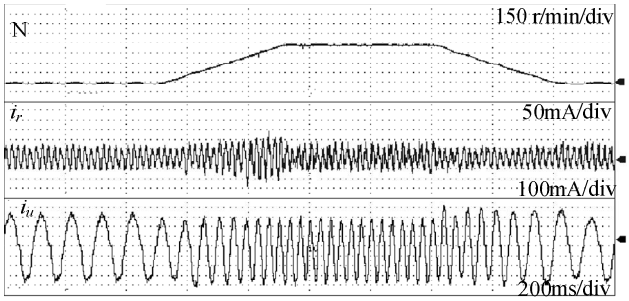

(b) Proposed converter.

Fig.16 Acceleration and deceleration characteristic.

This section demonstrates the speed characteristic of the induction motor under two different setups, normal mode and HEV mode. This experiment was conducted under a no-load condition. For the acceleration, the speed command increases from 300 r/min to 900 r/min. For the deceleration, the speed command decreases from 900 r/min to 300 r/min.

Fig. 16(a) shows the IMC only (normal mode) data. During acceleration, large input power is required until the speed is constant. The output current i_u shows a good sinusoidal waveform and the change of the shape of the frequency is due to the acceleration and deceleration control.

Fig. 16(b) shows the proposed circuit speed characteristic. When the motor speed is low (300 r/min), the battery current is set at 0 A. Once the acceleration starts, the battery power supplies 200 W immediately. Therefore, during acceleration the input current i_r has a low magnitude because the battery power is used to drive the motor instead providing the input power. When the speed is constant, the battery power continues delivering and the input power drops to the minimum.

Comparing Fig. 16(a) and Fig. 16(b), it can be seen that the output current i_u shows a perfect sinusoidal waveform. That is, the connection of the neutral point of the motor for using the boost converter does not affect the motor performance. Furthermore, the results demonstrate good control of the power management with the input and the battery.

5.5 Loss Analysis and Motor Efficiency

Fig. 17 shows the comparison of the losses among the conventional methods and the proposed method. The simulation parameters are the same as those listed in Table I. The battery current is controlled to 1 A. To clarify the advantage of the proposed method (b), the conventional method is operated at two frequencies: (a) 20 kHz and (c) 40 kHz. In this figure, P is the primary side, S is the secondary side and B is the boost converter. The conduction loss for the secondary side remains unchanged in the three results. Comparing (a) and (b), the switching loss is increased by 70%. However, comparing (a) and (c), the switching loss is increased by 95%, which is higher than that of the proposed method. As for the boost converter, comparing (a) and (b) shows approximately a 40% increase, but comparing (a) and (c) shows approximately a 87% increase. Overall, the total loss for (a) is 31 W, (b) is 37 W, and (c) is 41 W. The proposed method is able to achieve high efficiency and also to reduce the ripple in the battery current.

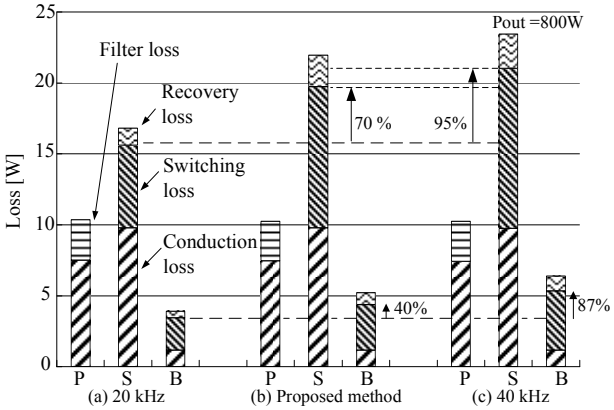

Fig. 17 Loss comparison among conventional methods and proposed method.

Studies on motor losses were also investigated by the authors. (See Refs. [13]-[14].) In the present proposed method, the battery current is added to the output current; therefore, the copper loss is increased proportionally. However, the copper loss in the rotor side remains unchanged because the zero-phase current (battery current) does not produce flux to rotate the rotor. Refs. [13] and [14] are studies of an internal permanent magnet (IPM) motor, where the copper loss is increased by 26% compared to that of the proposed method and the conventional method. The copper loss of the induction motor is also considered to increase. The studies show a trade-off relationship of the efficiency between the converter and the motor.

6. Conclusion

A simple high-frequency PWM method is proposed to reduce the ripple in the battery current. The simulation and experimental results confirm the validity of the proposed method. In addition, this paper discusses the performance of an induction motor, in which the neutral point of the motor is connected to a DC boost converter. Several experimental results showed that the motor works well, and even the stator leakage inductance is utilized in the boost converter.

(Manuscript received -. -, 2010, revised - -, 2010)

References

(1) Lixiang Wei; Lukaszewski, R.A; Lipo, T.A: "Analysis of Power- Cycling Capability of IGBT Modules in a Conventional Matrix Converter", IEEE Transactions on Industry Applications, Vol. 45, Issue. 4, pp. 1443-1451, June 2009

(2) Sahoo, A.K.; Meenakshi, J.; Dash, S.S; Thyagarajan, T : "Anlysis and simulation of matrix converter using PSIM", 7th International Conference on Power Electronics, pp.414-419, Oct 2007

(3) Shapoval, I.;l Clare, J.; Chekhet, E.: "Experimental study of a matrix converter excited doubly-fed induction machine in generation and motoring", 13th Power Electronic and Motion Control Conference, Poznan, pp. 307-312, Sept 2008.

(4) Itoh, J.-I.; Tamura, H.: “A Novel Control Strategy for a Combined System Using both Matrix Converter and Inverter without Interconnection Reactors.”, *Power Electronics Specialists Conference*, Rhodes, pp. 1741-1747, June 2008.
(5) Pena, R.; Cardenas, R.; Reyes, E.; Clare, J.; Wheeler, P.: “Control Strategy of an Indirect Matrix Converter with modifying DC voltage”, *13th European Conference on Power Electronics and Applications*, Barcelona, pp. 1-8, Sept. 2009.
(6) Gang Li; Kai Sun; Lipei Huang; Seiki Igarashi;: “RB-IGBT Gate Drive Unit and its Application in Two-Stage Matrix Converter”, *23th Annual IEEE in Applied Power Electroncis Conference and Exposition*, Austin, TX, pp. 245-251, Feb 2008
(7) Kato, K; Itoh, J-i.: “Control Strategy for a Buck-boost Type Direct Interface Converter using An Indirect Matrix Converter with an Active Snubber”, *Twenty-Fifth Annual IEEE Applied Power Electronics Conference and Exposition (APEC)*, Palm Springs, CA, pp. 1684-1691, Feb 2010
(8) Goh Teck Chiang; Itoh, J. –i.: “A Three-port Interface Converter by Using an Indirect Matrix Converter with the Neutral Point of the Motor”, *IEEE Energy Conversion Congress and Exposition*, San Jose, CA, Sept. 2009
(9) Itoh, J.; Sato, I.; Odaka, A.; Ohguchi, H.; Kodatchi, H.; Eguchi, N.: “A Novel Approach to Practical Matrix Converter Motor Drive System with Reverse Blocking IGBT”, *IEEE 35th Annual Power Electronics Specialist Conference*, Vol. 3, pp. 2380-2385, June 2004.
(10) Tsuji, M.; Xiaodan Zhao; He Zhang; Hamasaki, S.-I.; Shuo Chen: “Steady-state and Transient Characteristics of a Novel V/f Controlled Induction Motor”, *International Conference on Electrical Machines and Systems*, pp. 1-6, Nov. 2009
(11) Chen Wei; Yang Rong Feng; Yu Yong; Wang Gao Lin; Xu Dian Guo;, “A Novel Stability Improvement Method for V/F Controlled Induction Motor Drive Systems”, *International Conference on Electrical Machines and Systems*, Wuhan, pp. 1073-1076, Oct. 2008.
(12) Kato, K; Itoh, J-i.: “Control Method for a Three-Port Interface Converter using an Indirect Matrix Converter with an Active Snubber Circuit”, *13th Power Electronics and Motion Control Conference*, Poznan, pp.581-588, Sept. 2008
(13) Itoh, J-i., Ikarashi, D.: “Investigation of a two-stage boost converter using the neutral point of a motor”, *International Power Electronics Conference (IPEC)*, Sapporo, pp. 1180, 21-24 June 2010
(14) Itoh, J-i., Ikarashi, D.: “Loss evaluation of a two-stage boost converter using the neutral point of a motor”, *IEEE Energy Conversion Congress and Exposition (ECCE)*, Atlanta, GA, pp. 2600, 12-16 Sept. 2010

Goh Teck Chiang  (Student member) received his B.S. degree in electrical and electronic engineering from Queensland University of Technology, Brisbane, Australia in 2004 and his M.S. degree in electrical and electronic engineering from Nagaoka University of Technology, Japan in 2009, where he is currently working towards to a Ph.D. degree in electrical and electronic engineering. His research interests include indirect matrix converters and PWM.

Jun-ichi Itoh  (Member) received his M.S. and PhD degrees in electrical and electronic systems engineering from Nagaoka University of Technology, Nagaoka, Japan in 1996 and 2000, respectively. From 1996 to 2004, he was with Fuji Electric Corporate Research and Development Ltd., Tokyo, Japan. Since 2004, He has been with Nagaoka University of Technology as an associate professor. He received the IEEJ Academic Promotion Award (IEEJ Technical Development Award) in 2007. His research interests include matrix converters, DC/DC converters, power factor correction techniques and motor drives. He is a member of the Institute of Electrical Engineers of Japan.